pIJMT. Vol. 22, Iss. 1, 2026. (32-47)

International Journal of Maritime Technology

Journal homepage: ijmt.ir

Reconciling Per-Capita Water Metrics with Aquifer Stress on Qeshm Island: Pathways for Coastal Blue Economy Development

Emad Mahjoobi[1*], Mahan Azizi[2], Mohammadreza Asli Charandabi[3]

[1*] *Assistant Professor, Department of Water and Environmental Engineering, Faculty of Civil Engineering, Shahrood University of Technology, Shahrood, Iran, emahjoobi@shahroodut.ac.ir*
[2] *PhD student in Water Resources Engineering and Management, Faculty of Civil Engineering, Shahrood University of Technology, Shahrood, Iran, mahan.azizi@shahroodut.ac.ir*
[3] *PhD student in Water Resources Engineering and Management, Faculty of Civil Engineering, Shahrood University of Technology, Shahrood, Iran, m.aslicharandabi@shahroodut.ac.ir*

ARTICLE INFO

Article History:
Received: 22 Aug 2025
Last modification: 13 Nov 2025
Accepted: 15 Nov 2025
Available online: 17 Nov 2025

Article type:
Research paper

Keywords:
Groundwater Overdraft,
Qeshm Island Aquifer,
Renewable Water per Capita (RWRPC),
Salinization,
Water Scarcity Management

ABSTRACT

Qeshm Island's extreme aridity and rapid growth expose a mismatch between headline per-capita renewable water figures and actual aquifer stress. Using multi-decadal precipitation, census, and well records, we estimate renewable supply, recharge, storage, and salinity. Natural replenishment is minimal: about 60% of rainfall is lost to evaporation and most of the remainder leaves as runoff, yielding little effective recharge. Under trend-based demographic projections, renewable water per capita declines to 757 m^3 per person per year by 2036 (medium evaporation-loss scenario). Groundwater observations show a long-term water-table decline near 0.091 m per year and salinity rising to about 14 to 16.6 dS/m, consistent with persistent overdraft and seawater intrusion or up-coning. To translate hydrologic limits into development choices, we evaluate a conservative 40% withdrawal of renewable yield with a mixed allocation 70% agriculture, 20% industry, 10% domestic. At this intensity the budget can irrigate about 1,523 ha of date palms, support roughly 335,000 t/yr of petrochemical output, and supply about 23,841 residents, generating approximately $16.45 million (agriculture), $334.69 million (industry), and $0.22 million (domestic) per year around $351 million in total. These results show that per-capita indicators alone can overstate security; resilient coastal-marine development on Qeshm will require aligning withdrawals with limited renewability and storage, coupled with managed aquifer recharge, targeted desalination, and selective use of saline groundwater to protect potable supplies and industrial applications requiring low-salinity makeup water (e.g., boiler and cooling systems), where acceptable conductivity is typically $\lesssim$0.2–2 dS m^{-1} with low hardness and silica.

ISSN: 2645-8136

DOI:

1. Introduction

The Water is vital for drinking, agriculture, sanitation, energy, and ecosystems, yet global per capita renewable water resources are declining under the combined pressures of population growth, climate change, urbanization, and rising demand [1]; [2]. This per capita renewable water metric now serves as a crucial warning of impending shortages. The apparent contradiction between increasing per capita renewable water projections and worsening local aquifer conditions, specifically groundwater overdraft and salinization, is a growing concern in hydrological research and water resource management. This studysynthesizes findings from recent studies to examine how this disconnect occurs, the underlying processes contributing to groundwater degradation, and possible solutions for reconciling projections with aquifer realities. Many national and regional water assessments rely on per capita renewable freshwater estimates, which often overlook local groundwater stress. For instance, projections for the Arab region show that groundwater per capita is expected to decrease by over 50% by 2050 due to population growth and over-extraction. However, these projections fail to account for the depletion of aquifers from which over 88% of irrigation withdrawals are made [3]. Similarly, in Beijing, renewable water modeling obscures severe groundwater overuse and contamination from agricultural runoff and rapid urbanization [4]. The same discrepancy is evident in the Central Valley of California, where despite the appearance of moderate regional water availability, groundwater storage has declined by approximately 3 km^3 annually, with the overdraft intensifying during drought periods [5]. This trend is illustrated in regions worldwide. In Jordan, rapid population growth outpaced its limited renewable supply by the 2010s, forcing reliance on imports and desalination [6]. India's per capita availability fell from over 5,000 m^3 in 1950 to under 1,500 m^3 by 2006 [7]. In Iran and Turkey, over-extracted aquifers, inefficient irrigation, and reduced rainfall intensify stress [8]. In a study conducted on the Guinea Savanna ecological zone of Nigeria, the impacts of climate change and population growth on water resources were analyzed. The researchers identified declining rainfall, increasing temperatures, and rapid population growth as major stressors leading to seasonal water shortages and growing demand for agricultural and domestic water use. Using data from the Nigerian Meteorological Agency and the National Population Commission, the study revealed significant environmental changes and demographic pressures that threaten sustainable water access in the region. To mitigate these risks, the authors recommend integrated water resource management, afforestation, climate-resilient agriculture, and policy-driven awareness programs [9] Not all trends are downward. Many OECD nations have decoupled water use from GDP through efficiency gains, service-oriented economies, effective pricing, and conservation policies [10];[11]. California's tiered pricing and sustained behavior changes cut daily residential use even post-drought [12]; [13]. Such efficient appliances, land-use planning, and lasting habit shifts can "bend the curve" of per capita demand [14]. Aquifer overdraft is largely driven by unsustainable agricultural withdrawals. In Libya's Jifarah Plain, decades of unregulated pumping have resulted significant seawater intrusion, converting previously fresh groundwater into saline-dominated regimes [15]. Similar issues are observed in the Chicot Aquifer in Louisiana, where overdraft has resulted in an increased extent of saltwater-affected zones, especially during drought years [16]. Groundwater salinization, often a consequence of overdraft, is a pressing problem in many coastal and arid aquifers. In the Canary Islands, a combination of airborne salt, irrigation return flow, and limited recharge has significantly increased aquifer salinity levels [17]. The Motril-Salobreña aquifer in Spain similarly demonstrates long-term anthropogenic and natural influences, including sea-level changes, that have disrupted historical recharge regimes and led to new saline equilibria [18].

One of the most promising strategies to address overdraft and salinization is Managed Aquifer Recharge (MAR). In California's Tulare and San Joaquin Basins, if properly implemented, MAR using excess winter flows could recover 30%–60% of the existing groundwater deficit [5]. Recharge projects placed over geologically favorable zones (e.g., incised valley fills) significantly improved groundwater quality and reduced salinity migration [19]. Innovative policy tools have also emerged. The Pajaro Valley's Recharge Net Metering (ReNeM) program incentivizes private landowners to develop recharge infrastructure, offering rebates for infiltration volumes and improving regional aquifer conditions [20]. Simulations indicate that artificial recharge In Sacramento's Lower American River Basin could offer both environmental and economic co-benefits, including hydropower gains and reduced water scarcity costs [21].

Even with promising technical solutions, practical implementation faces barriers. In Spain, groundwater rights and user resistance have hindered the effectiveness of MAR and desalination-based offset schemes [22]. Saltwater intrusion exacerbated by reduced recharge and climate-induced sea-level rise is a growing concern in coastal India. Under anticipated overdraft scenarios, more than two-thirds of the aquifer could exceed safe salinity limits [23]. In Southeast Spain, groundwater overdraft has reached critical levels, and even with the introduction of desalinated seawater as an alternative, economic and logistical barriers have limited its effectiveness in reducing aquifer stress [24].

Iran's case is stark: agriculture consumes over 90% of withdrawals yet yields low economic return, prompting growing virtual water imports of staples like wheat [25]. GRACE satellite data reveal a loss of 211 km³ in total water storage from 2003 to 2019 double annual consumption driven chiefly by groundwater overuse despite some precipitation gains [26]. System-dynamics models confirm that recurrent droughts, warming, and population growth sharply curtail renewable supplies [27]; [28], and water security indices fell consistently across major Iranian basins from 1996 to 2016 [29]. Efforts to reduce per capita use in arid coastal zones have delivered only modest gains but large-scale solar-powered desalination offers a promising supply-side solution for provinces such as Hormozgan [23].

Qeshm Island, located in the Persian Gulf near the Hormoz Strait, is part of the Zagros sedimentary-structural unit and has a significant impact on the surface and underground water resources quality. The island, with an area approximately 1,491 km², lacks permanent rivers but has several watersheds, including Tourian, Pay Posht, Deirestan, Gowdrin, Giahdan, and Ramchah. The average annual volume of runoff water is approximately 37 million m³. The primary aquifer on the island is located in the Tourian plain, with additional scattered aquifers in areas such as Deirestan, Tonban, Soheili, Table, Gavarzin, Tourgan, and Laft. Annually, 4-8 million m³ of surface water and up to 3 million m³ of underground water are utilized, leading to a negative water balance in recent years. The water quality is generally medium to good, and 387 wells and various storage methods, including earth barriers, dams, and water reservoirs are used. To address water supply and quality maintenance, suggestions include optimal management of current resources, exploration of new underground water resources, seawater desalination, water transfer from the mainland, and proper sewerage collection and treatment [30].

The vulnerability of the Tourian aquifer was assessed using the SITE index (including chloride concentration), and future vulnerability was predicted using an ARIMA (2,1,1) model with a mean absolute error of 13.3 mg/L and a Nash–Sutcliffe efficiency of 0.81. Results indicated moderate vulnerability overall, with 0.95 km² classified as high vulnerability, and a rising trend over time. Sensitivity analysis showed the model was particularly sensitive to surface affected (S) and intensity of intrusion (I) underscoring the need for careful monitoring and management of these factors [31].

The main objective of this article is to analyze the long-term rainfall on Qeshm Island and the long-term changes in per-capita renewable water on the island, as well as to examine the existing groundwater resources to assess the island's development capacity and determine how long its current water resources can sustain it. This study analyzes historical climate and demographic data, water availability trends, and socio-environmental factors to uncover the drivers and impacts of water resource depletion and develop sustainable management strategies tailored to this vulnerable coastal microcosm.

Beyond hydrologic accounting, this study addresses a coastal-engineering problem: managing a Gulf-margin coastal aquifer under hyper-arid climate, rising salinity, and minimal natural recharge. We interpret head and salinity trends in the context of seawater intrusion pathways (lateral encroachment and vertical up-coning), evaluate allocation strategies under a sustainable-use cap, and outline marine-adjacent interventions—including subsurface intakes, hydraulic barriers, and managed aquifer recharge (MAR) using treated wastewater—that align groundwater stewardship with the island's sea-oriented development.

2. Material and Methods

2.1. Study Area

The study area focuses on Qeshm Island, the largest of Hormozgan Province's northern Persian Gulf islands (Figure 1). Situated just off the strategic Strait of Hormuz, Qeshm Island exhibits varied morphology from coastal plains to rugged highlands and is characterized by an arid climate with scant rainfall, minimal catchment areas, and high evaporation rates that severely limit freshwater availability. Qeshm Island covers an area of 1,491 km². Its resident population has increased across recent censuses, from 32,457 in 2006 to 41,981 in 2011 and 62,177 in 2016. population and water demand on Qeshm continue to grow, securing a sustainable freshwater supply has become critical.

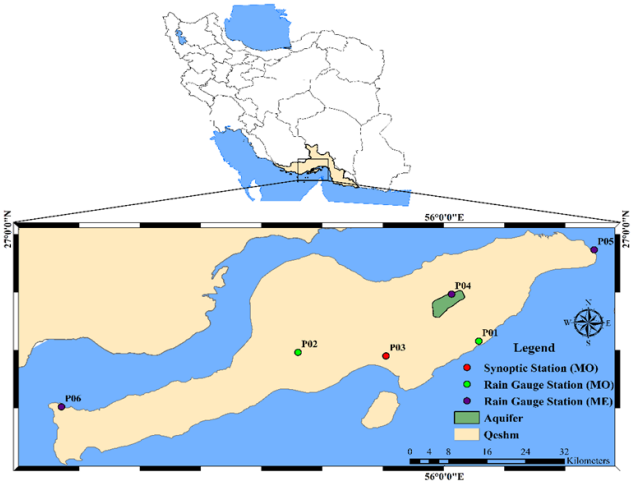

Figure 1. Study area on Qeshm Island showing the the aquifer, and monitoring network

The Qeshm Island coastal aquifer faces critical challenges from seawater intrusion and declining recharge rates [32]. Hydrogeological studies have revealed water table depths shallower than 5 m in

northern sectors, with chloride concentrations exceeding 2500 mg/L in 68% of the monitored wells [33]. The GALDIT model assessments have demonstrated severe seawater intrusion vulnerability along 83% of the coastline, particularly in the southeastern plains [34]. Numerical modeling confirms an annual freshwater loss of 12% due to over-extraction, recommending managed aquifer recharge as the most viable mitigation strategy [35]. In this study, we employed Piezometric and Monitoring wells to assess the groundwater characteristics in the study area. Piezometric wells were used as quantitative monitoring points to measure hydraulic parameters, including water depth, wellhead elevation, and water table levels. Meanwhile, Monitoring wells served as qualitative monitoring stations to evaluate the groundwater quality through chemical analysis. Figure 2 shows the spatial distribution of these quantitative (Piezometric) and qualitative (Monitoring) wells across the study area. Table 1 presents the quantitative and qualitative characteristics of the wells used within the Qeshm aquifer. It should be noted that well-specific or aggregated pumpage records were not available; overdraft was therefore inferred from the observed head-decline calibration. The implication is that Q_{eff} reflects net stress (withdrawals minus recharge); tighter bounds would require pumpage reporting.

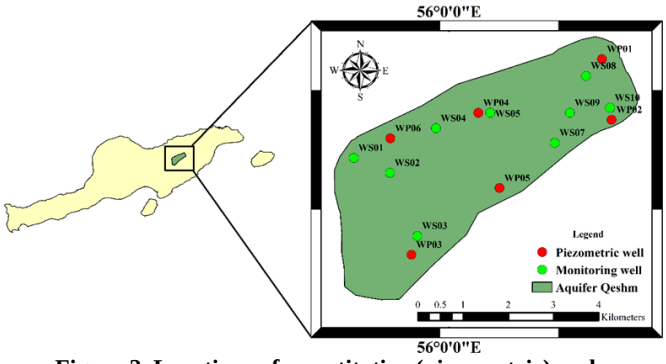

Figure 2. Locations of quantitative (piezometric) and qualitative (monitoring) wells within the Qeshm aquifer

2.2. Data collection

To quantify the availability of renewable water, we assembled long-term precipitation and population records. Precipitation data cover the mid-1990s to 2024 (water years 1994–95 through 2023–24, defined as October–September) from 6 rain gauges and synoptic stations, both coastal and island, maintained by the Islamic Republic of Iran Meteorological Organization (IRIMO) and the Hormozgan Regional Water Authority (Table 2). Island population counts were drawn from the 2006, 2011, and 2016 national censuses (Statistical Center of Iran) and supplemented with local administrative records, providing benchmarks at the start, middle, and end of the study's first two decades.

Table 1. Monitoring and Piezometric characteristics of the wells in the Qeshm aquifer

	Well ID	Latitude	Longitude	EC (µS/cm)
Monitoring Wells	WS01	55.98	26.86	18126.4
	WS02	55.99	26.85	20378.7
	WS03	55.99	26.84	23856.1
	WS04	56.00	26.86	14157.1
	WS05	56.01	26.87	8366
	WS06	56.01	26.86	7268.29
	WS07	56.02	26.85	13852.4
	WS08	56.03	26.87	3238.18
	WS09	56.03	26.88	7697.69
	WS10	56.04	26.86	9841.94
	Well ID	Latitude	Longitude	Water Table Elevation (m)
Piezometric Wells	WP01	56.0304	26.8757	2.98
	WP02	56.0323	26.8636	-4.58
	WP03	55.9925	26.8367	-3.11
	WP04	56.0058	26.865	-29.55
	WP05	56.01	26.85	-6.93
	WP06	55.9883	26.8599	-16.79

Table 2. Meteorological station metadata

Assigned name	Station name	Type	Longitude	Latitude	Elevation(m)	Mean annual precipitation
P01	Sooza	Rain Gauge	56.06	26.78	13	73.94
P02	Tabl	Rain Gauge	55.73	26.76	0	86.17
P03	Qeshm Island	Synoptic	55.89	26.75	6	114.38
P04	Torian-E.Qeshm	Rain Gauge	56.01	26.87	20	148.22
P05	Qeshm	Rain Gauge	56.28	26.96	18	184.57
P06	Basaiedo	Rain Gauge	55.29	26.65	10	78.66

The dataset comprises 6 piezometers (WP01–WP06) for heads, 10 monitoring wells (WS01–WS10) for water quality, and 6 precipitation stations (P01–P06). Using great-circle (haversine) distances on WGS84 coordinates, nearest-neighbor spacing is 1.36–2.28 km (median 1.72 km) for piezometers and 0.99–1.49 km (median 1.11 km) for quality wells over the 17.2 km² aquifer; the rainfall network spans the island with

spacing 11.2–45.4 km (median 15.9 km). Areal densities are ~35 (piezometers) and ~58 (monitoring wells) per 100 km² over the aquifer, and ~0.40 rain/synoptic stations per 100 km² at the island scale (~1,493 km²). This is adequate for basin-scale diagnostics (aquifer-wide trends, coastal–inland contrasts).

Given the presence of a groundwater aquifer within the Qeshm Island area, the total renewable water resources on Qeshm Island were estimated by combining precipitation and runoff data from the Iran Meteorological Organization and the Ministry of Energy with groundwater records provided by the Ministry of Energy. Hydraulic (Piezometric) well data were available for the from 2002 to 2018, whereas chemical (Monitoring) well data were available from 2006 to 2019. The water-quality dataset comprised measurements of electrical conductivity (EC). We estimated water column depth, well-rim elevation, and groundwater-table elevation for each hydraulic well. The study area encompasses six Piezometric wells and ten Monitoring wells.

2.3. Method

Open-water surfaces evaporate far more than land-1,200–3,200 mm yr⁻¹ versus a global terrestrial average of ~549 mm yr⁻¹-because oceans and seas offer unlimited moisture, greater heat capacity, and stronger mixing than vegetated or arid land does not [36]; [24]. Worldwide, approximately 86% of evaporation comes from oceans and seas and only 14% from land. In Iran's dry climate, approximately 68% of rainfall is lost before it can recharge storage or aquifers [28].

To estimate renewable water per capita , we subtract an evaporative loss E (65%, 70%, or 75% of annual precipitation) from P, multiply by island area A (km², converted to m³), and divide by population Capita: (Notation: We denote renewable water per capita as RWRPC (m³ person⁻¹ yr⁻¹) and use it consistently hereafter.)

$$RWRPC = \frac{(P - E) \times A}{Capita} \quad (1)$$

Here, the three scenarios leave 35%, 30%, or 25% of *P* available per year per capita under increasing conservatism. Equation (1) yields the maximum annual renewable water per person under a given evaporation loss and follows global assessment standards (Jiang, 2015). We benchmark RWRPC against Falkenmark thresholds>2,500 m³ pp yr⁻¹ (vulnerability), 1,700 m³ (stress), 1,000 m³ (scarcity), and 500 m³ (absolute scarcity) (Falkenmark et al., 1989; Gain et al., 2025))to classify islands' water-stress levels and development capacity.

The annual Island precipitation (water years 1994–95 to 2023–24) was interpolated from six coastal and island stations using Thiessen polygons to produce a 29-year series.

Basin-wide annual indicators (RWR, RWRPC, composite EC and head) use Thiessen weighting to average station/well values. As a robustness check, island-average precipitation was also computed with Inverse Distance Weighting (IDW) and ordinary kriging (OK); differences were minor and do not affect category assignments. Given the small number of wells, we do not produce kriged maps of heads or EC; instead, we report (i) trend statistics (MK/Sen) on Thiessen-aggregated series and (ii) per-well trends for representativeness, and we analyze coastal proximity and head relative to mean sea level for mechanism (lateral intrusion vs. up-coning).

Population counts from the 2006, 2011, and 2016 censuses were linked by exponential interpolation and were extended to 2024 using provincial growth rates and development plans. We implemented an exponential growth projection calibrated to the 2006, 2011, and 2016 censuses using nonlinear least squares to estimate a constant rate *r*. We then produced a hybrid projection: (i) a trend-based extrapolation $C_t = C_{2016}\, e^{r(t-2016)}$ and (ii) a policy-constrained variant in which r is capped to the provincial five-year development targets for Hormozgan. The headline 2036 population (71.8k) corresponds to the trend-based case.

Applying each of the three evaporation scenarios (65%, 70%, and 75% loss), we computed the yearly RWRPC for Qeshm Island, compared them to the Falkenmark categories, and identified those beyond the sustainable carrying capacity or with room for growth.

We adopt a 70/20/10 policy benchmark (agriculture / industry / municipal) because global assessments consistently show that agriculture accounts for about 70% of freshwater withdrawals, with industry near 20% and municipal about 10–12%. The UNESCO/UN-Water World Water Development Report 2024 reports "agriculture ~70%, industry just under 20%, and domestic about 12%" at the worldwide scale, a pattern used widely in comparative planning [37]. The FAO AQUASTAT methodology the primary statistical backbone for sectoral withdrawal shares used by UN agencies likewise reports 69% agricultural, 19% industrial, and 12% municipal at the global level [38]. Peer-reviewed syntheses align with this distribution; for example, Ingrao et al. (2023) notes that agriculture is responsible for nearly 70% of global freshwater withdrawals, with industry and domestic uses accounting for the remainder [39]. Given these convergent lines of evidence, we use 70/20/10 as a neutral, data-anchored baseline for scenario analysis, while recognizing that local shares can deviate from the global mean.

The volume of renewable water can be estimated directly as the product of annual rainfall, catchment area, and an infiltration (runoff) coefficient commonly taken as ≈ 40% in coarse-grained arid catchments

[40];[41] without determining the total aquifer storage. In other words, if the mean annual rainfall is P and the catchment area is *A*, then the annual recharge volume is as follows:

$$V_{recharge} = C \times A \times P \quad (2)$$

The total aquifer storage volume, $V_{recharge}$ is the volume of water stored in the aquifer that is available for withdrawal, expressed in cubic meters. With the unit conversion 1 mm·km² = 1 000 m³ [42], this value can be readily expressed in cubic meters. This simple water-budget approach provides a robust basis for setting a sustainable long-term withdrawal rate without the need for detailed knowledge of pore-volume or complex storage parameters [41]; [43] C is the dimensionless infiltration (or recharge) coefficient, representing the fraction of precipitation that actually percolates into groundwater past the root and evaporation zones; its value ranges from 0 (no recharge) to 1 (all rainfall recharges), and in arid catchments, it often lies between 0.1 and 0.6. A denotes the catchment area, which is the surface area over which rainfall is collected and can contribute to recharge, usually measured in km² or ha. P is the depth of the mean annual precipitation (or rainfall) over the catchment, expressed in millimeters per year; it drives the potential recharge before accounting for losses. Total aquifer storage:

$$V_{storage} = S \times B \times A \quad (3)$$

S is the storativity (or storage coefficient), a dimensionless parameter that quantifies the volume of water that an aquifer releases (or stores) per unit surface area per unit change in the hydraulic head; for confined aquifers, S_b is the storativity of a confined aquifer, a dimensionless measure of how much water a confined aquifer releases from, or takes into, storage per unit area for a unit change in hydraulic head. It is governed by the elastic compressibility of both the aquifer skeleton and the pore water together with the saturated thickness. Typical ranges are about 10^{-5} to 10^{-3} and for unconfined aquifers. S_y is the specific yield of an unconfined aquifer, a dimensionless drainable porosity, defined as the fraction of the saturated water that drains under gravity as the water table falls (and is refilled as it rises). It primarily depends on material texture (higher in sands and gravels, lower in silts and clays). Typical ranges are about 0.05 to 0.30, and this term usually dominates storage changes in unconfined aquifers. *B* represents the saturated thickness of the aquifer and the vertical thickness (in m) of the water-bearing formation, which directly scales the storage capacity. *A* is the aerial extent of the aquifer (in m² or km²), used to convert the storage coefficient into total volumetric storage.

To estimate the support horizon under the current net stress, the storage volume is divided by the net depletion (overdraft) rate:

$$T = \frac{V_{storage}}{Q_{overdraft}} \quad (4)$$

The number of years of support (*T*) quantifies how long stored groundwater can sustain the current net depletion, computed as the ratio of recoverable storage to the net overdraft. Here $Q_{overdraft}$ denotes the annual withdrawals minus natural recharge (m³ yr^{-1}); it sets the rate at which storage is drawn down.

For consistency with observed heads, the net depletion was calibrated from the groundwater-level trend using the baseline aquifer properties:

$$Q_{overdraft} \approx S_{y,base} \times A \times \Delta h \quad (5)$$

Equation (5) preserves the empirically inferred net stress while S_y and *B* are perturbed in the sensitivity analysis mentioned later in this section. Plus, Because the baseline decline-calibrated $Q_{overdraft}$ effectively reflects net depletion under negligible recharge, we also test small, literature-consistent recharge inputs by holding withdrawals constant and crediting a minimal recharge $R = \varepsilon AP$ with ε being 1-2% of rainfall. The effective depletion becomes $Q_{eff} = Q_{overdraft} - R$, and the support time is recomputed as $T = V_{storage}/Q_{eff}$. This treatment reflects evidence that in hyper-arid settings diffuse recharge is typically very small, with effective recharge occurring mainly as episodic, focused wadi infiltration; hence $R = \varepsilon AP$ is used only as a small positive bound *[44]*.

The next step would be sensitivity analysis. Parameter uncertainty was propagated to $V_{storage}$ and T by sampling $S_y \in [0.18, 0.43]$ in increments of 0.01 and $B \in [15, 40]$ m in increments of 1 m and also, testing minimal-recharge cases $R = \varepsilon AP$ with $\varepsilon = 1\%\ and\ 2\%$. For each pair ($S_y$, *B*)(and ε), $V_{storage} = S_y \times B \times A$ is computed and the corresponding support time (*T*) is evaluated at the observed decline rate via Eq. (4) with $Q_{overdraft}$ from Eq. (5) (or $Q_{eff} = Q_{overdraft} - R$ for the minimal-recharge cases). Results are reported as (i) a compact set of scenarios, (ii) a one-at-a-time summary (tornado plot), and (iii) the two-parameter response surface *T*(S_y, *B*) (contour map). This procedure quantifies the sensitivity of storage and support time to plausible ranges in aquifer properties while remaining anchored to the measured long-term decline.

Afterwards, For each monitoring well, we associated EC observations with the nearest piezometer (by geographic coordinates) to examine (i) EC versus head relative to mean sea level (MSL) and (ii) spatial coastal gradients. Piezometric heads are reported in meters relative to MSL (negative = sub-MSL). EC values were treated as µS cm^{-1} and, where needed, expressed as dS m^{-1} using 1 dS m^{-1}=1000 µS cm^{-1}. Wells with elevated EC colocated with sub-MSL heads were flagged as lateral intrusion candidates; inland sites where EC increases while adjacent heads remain above MSL

were flagged for possible up-coning from deeper saline layers.

Lastly, We tested trends in groundwater level and electrical conductivity (EC) using the Mann–Kendall (MK) non-parametric test with Sen's slope and 95% confidence intervals (Helsel–Hirsch approach). Monthly data were aggregated to annual means prior to testing. We report results for the Thiessen-aggregated (aquifer-wide) series, and for individual wells where ≥8 annual observations were available. Tests are two-sided at $\alpha = 0.05$. For EC, values were treated as µS cm^{-1}; where helpful we also express slopes in dS m^{-1} yr^{-1} using 1 dS m^{-1}=1000 µS cm^{-1}.

3. Results and discussion

3.1. Rainfall Characteristics

Qeshm Island lies within the Persian Gulf's hyper-arid dryland belt, as documented by Lazzarini et al. for Gulf hot-desert, hyper-arid settings *[45]*, and by Holocene–present syntheses that explicitly describe the Persian Gulf as a hyper-arid region *[46]*. Table 3 presents a statistical summary of the annual precipitation on the island studied during the analysis period.

Table 3. Statistical summary of annual precipitation (island-mean, Thiessen)

	Min	Avg	Max	STD	CV
Annual precipitation (mm)	2.19	121.59	546.37	107.73	0.89

On Qeshm Island, the average annual rainfall is extremely low roughly 106 mm in its driest years and up to appproximately 175 mm in its wettest compared with ~250 mm nationally in Iran and ~800 mm globally. Year-to-year variability is pronounced: the coefficients of variation of precipitation often exceeds 0.75, reflecting extremes from virtually no rainfall in dry years to heavy downpours in wet ones. Even when rain does fall, intense heat and scant vegetation mean that much of it evaporates before it can be captured. These figures underscore that Qeshm Island faces severe and highly erratic water scarcity.

3.2. Population Growth and Water Availability Per Capita

Population growth on Qeshm Island has compounded its scant, erratic rainfall to sharply reduce per-person water supplies. Between 2006 and 2016, Qeshm's population rose from 32,457 in 2006 to 62,177 in 2016 (a 91% increase). As a result, nearly twice as many residents now share any finite renewable water resources compared to the 1990s. Table 4 summarizes Qeshm's RWRPC statistics (1996–2023) under the 70% evaporation-loss scenario, highlighting a pervasive downward trend in water availability per-capita.

Table 4. Statistical summary of renewable water per capita (RWRPC) under 70 % loss

	Min	Avg	Max	STD	CV
Per capita renewable water resources (m^3/yr)	17	1252	5812	1200	0.96

On Qeshm Island, the average long-term RWRPC under the 70% evaporation-loss scenario is approximately 1252 m^3 pp yr^{-1}, placing it squarely in the "vulnerable" range. The time-series under the 70% evaporation scenario (Figure 3) shows a pronounced downward trend: in the late 1990s and early 2000s, wet years on Qeshm occasionally exceeded 1700 m^3 pp yr^{-1}, but even the highest annual values failed to reach that level by the 2010s. In recent years, Qeshm's RWRPC has stabilized below 1300 m^3 pp yr^{-1}. Without substantial storage infrastructure to capture wet-year surpluses, the island cannot buffer against prolonged dry spells. Our analysis finds that over 80 % of the decline in per capita water availability on Qeshm is driven by population growth rather than reduced rainfall, making demographic pressure the principal factor in its escalating water stress.

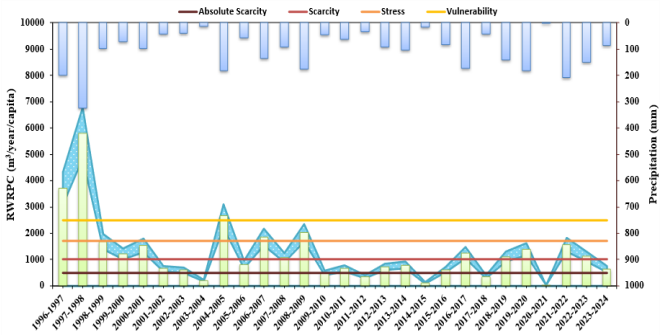

Figure 3. RWRPC and precipitation trends in Qeshm

Projecting the population of Qeshm Island to 2036 under current growth trajectories yields roughly 71800 residents. Under the medium (70%) evaporation-loss scenario, this drives the island's RWRPC down to about 757 m^3 yr^{-1} compared to its long-term average of ~1252 m^3 yr^{-1}. Without substantial imports or desalination, Qeshm will move deeper into the "scarce" water category by 2036, underscoring a stark mismatch between its development ambitions and the island's limited renewable water endowment.

3.3. Sectoral Water Use Capacity and Implications for Development

Under a conservative 40% extraction cap on the island's total renewable yield (RWR ≈ 54.4 × 10^6 m^3 yr^{-1}), the sustainable-use budget is $W_{sust} = 0.40 \times RWR = 21.75 \times 10^6\ m^3\ yr^{-1}$. Using the sector coefficients already adopted in this study—

$domestic\ \alpha_D = 0.365L = 0.365 \times 250 = 91.25\ m^3\ person^{-1}\ yr^{-1}$; $agriculture\ \alpha_A = 10{,}000\ m^3\ ha^{-1}\ yr^{-1}(date\ palms)$; $industry\ \alpha_I = 13\ m^3\ t^{-1}$ —the same water budget could support:

$$Domestic: N = \frac{W_{sust}}{\alpha_D} \approx 2.38 \times 10^5\ people,$$

$$Agriculture: H = \frac{W_{sust}}{\alpha_A} \approx 2{,}175\ ha,$$

$$Industry: Q = \frac{W_{sust}}{\alpha_I} \approx 1.67 \times 10^6\ t\ yr^{-1}.$$

For the 70/20/10 policy benchmark evaluated here, allocations are $W_A = 0.70W_{sust}$, $W_I = 0.20W_{sust}$, $and\ W_D = 0.10W_{sust}$. Mapping these volumes through the sector coefficients yields the capacities reported in Table 5. Revenues are computed transparently as, $V_A = p_A H,\ V_I = p_I Q,\ and\ V_D = p_D N$, using the same unit values across scenarios (back-calculated from the totals shown in Table 5): $p_A \approx 10{,}800\ USD\ ha^{-1}\ yr^{-1}$, $p_I \approx 1{,}000\ USD\ t^{-1}$, $p_D \approx 9.1\ USD\ person^{-1}\ yr^{-1}$. Monetary figures are gross and in constant USD of the analysis year. A ±25% price band shifts totals proportionally but does not change the comparative ordering of scenarios under the adopted water cap.

Table 5. Development potential across various sectors, global average allocation pattern, and resulting revenue in Qeshm Island

Expected Population_2036		71811
RWRPC_2036 (m^3/yr.capita)		757
RWR_2036 ($10^6 m^3$/yr)		54.39
40%RWR_2036 ($10^6 m^3$/yr)		21.75
Development Capacity	Domestic (Person)	238410
	Agriculture (hectare)	2175
	Industry (tonne)	1673453
Allocation Scenario	Domestic (Person)	23841
	Agriculture (hectare)	1523
	Industry (tonne)	334691
Income	Domestic ($)	217549
	Agriculture ($10^3$$)	16446.7
	Industry ($10^6$$)	334.69

Under a mixed-allocation scenario that devotes 70% of Qeshm's 40% sustainable-use cap to agriculture, 20% to industry, and 10% to domestic supply, the island's 21.75 × 10^6 m^3 yr^{-1} renewable resource could irrigate approximately 1523 ha of date palms, sustain roughly 334700 t yr^{-1} of petrochemical output, and meet the water needs of about 23841 residents. Financially, this allocation would generate an estimated $217549 from domestic sales, $16.45 million in agricultural revenues, and $334.69 million from industrial output. These projections demonstrate that, even with only a 10% share reserved for households, Qeshm's renewable water supply not only exceeds local demand by more than threefold but also supports substantial agricultural and industrial development underscoring the importance of integrated water management, strategic storage investments, and judicious allocation to secure the island's long-term water security.

3.4. Groundwater Conditions from the Piezometric and Monitoring of Wells

To characterize the state of the Qeshm Island aquifer, we analyzed two complementary datasets from the in-situ monitoring network: (1) Piezometric wells (six wells) providing annual aggregated water table elevations, and (2) Monitoring wells (ten wells) providing annual aggregated electrical conductivity (EC) as a proxy for salinity. The annual value of the respective parameter was extracted for each well, and spatial aggregation over the entire aquifer was performed using Thiessen polygon weighting to yield a single representative aquifer-scale value per year. Then, trend analyses were then applied to the time series to assess long-term changes.

The aggregated water table elevation shows a clear declining trend over the study period (Figure 4). Beginning approximately 10.5 m under sea level in 2002–2003, the water table progressively deepened to approximately 11.7 m under sea level by 2017–2018. A least-squares linear regression on the series indicates a decline of the order of ~0.091 m yr^{-1}, with a high coefficient of determination (R^2 indicative of a strong fit), reflecting sustained depletion. Interannual fluctuations are superimposed on this long-term decline, including a relative recovery around 2008–2010 and a transient rise in 2013–2014, followed by continued drawdown and a pronounced low in 2016–2017. These fluctuations likely reflect variability in recharge (e.g., from episodic precipitation), pumping rates, and possible short-term management or usage changes.

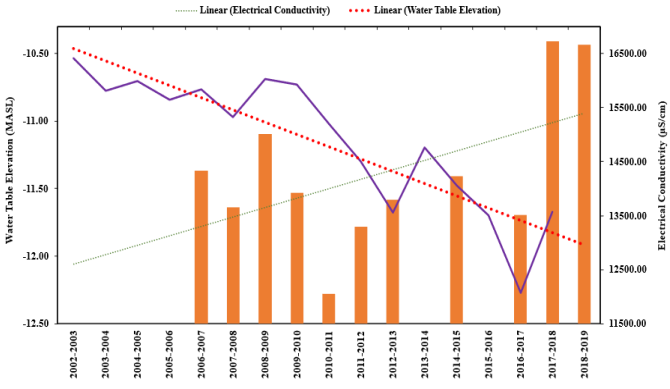

Figure 4. Combined time-series of annual means showing groundwater level and salinity trends in the Qeshm Island aquifer. The purple solid line (left axis; m relative to MSL (negative = sub-MSL) is the annual water-table elevation computed from six Piezometric wells (2002–2003 to 2017–2018); the orange bars (right axis; µS cm^{-1}) are the annual electrical conductivity from ten Monitoring wells (2006–2007 to 2018–2019). Overlaid linear regression trends (red dotted line for water-table elevation; green dotted line for electrical conductivity).

In contrast, the electrical conductivity time series (Figure 4) exhibits a general increasing trend across the aquifer, rising from roughly 14,300 µS/cm in 2006–2007 to over 16,600 µS/cm by 2018–2019, with peak values exceeding 16,600 µS/cm in the latest interval. The linear regression of EC yields an increase of approximately 150–170 µS/cm yr^{-1}, again with a strong fit (R^2 consistent with a meaningful upward trend). The EC escalation signals the progressive salinization of groundwater, consistent with the stressors on a coastal aquifer system.

The concurrent decline in water table elevation and rise in EC are suggestive of coupled processes: intensified groundwater extraction reducing hydraulic head can induce seawater intrusion or up-coning of deeper, more saline waters, particularly in a porous coastal setting like Qeshm Island. Reduced fresh recharge from climatic variability or land-use changes would intesify head declines and diminish the hydraulic barrier to saline encroachment. The intermittent rebounds in the water table (e.g., around 2013) that do not correspond to decreases in EC further imply that salinization exhibits inertia; they are not rapidly reversed by short-term water table recoveries once saline fronts advance. Figure 5 shows the Monitoring wells and Figure 6 depicts the Piezometric wells; they represent the annual average changes in electrical conductivity (EC) and the annual average changes in groundwater table elevation (GTE). The spatial patterns of long-term groundwater decline (from Piezometric wells) and salinization (from Monitoring wells) on Qeshm Island reveal coupled stress across the aquifer. The Piezometric-well interpolation shows the largest head declines in the central-northern (WP04) and western (WP06) sectors, whereas eastern and some south-central areas (WP01, WP02, WP05) exhibit little to no drawdown. Conversely, the Monitoring-well map displays a gradient of increasing salinity from northeast to southwest: the highest EC appears in the southwestern and western parts (e.g., WS03, WS01, WS02), while the northeast (WS08, WS09) retains comparatively lower salinity. The co-location of severe water table decline and elevated salinity in parts of the system, particularly in the west and central-north, suggests synergistic degradation likely driven by over-extraction, which lowers hydraulic resistance and facilitates saline intrusion or up-coning. These interacting Piezometric-Monitoring feedback amplify the risk of crossing irreversible thresholds in groundwater availability and usability.

The co-evolution of declining heads and rising EC shows spatial structure consistent with mixed mechanisms. Five out of six piezometers (WP02, WP03, WP04, WP05, WP06) register sub-MSL heads (−4.6 to −29.6 m), whereas WP01 is above MSL (+2.98 m). Monitoring wells closest to WP01 (WS08, WS09) show the lowest salinity (≈3.24 and 7.70 dS m^{-1}), while wells nearest to sub-MSL piezometers exhibit high EC (e.g., WS03 ≈ 23.86 dS m^{-1} near WP03; WS02 ≈ 20.38 dS m^{-1} near WP05/WP03; WS01 ≈ 18.13 dS m^{-1} near WP06/WP03; WS04 ≈ 14.16 dS m^{-1} near WP04; WS07 ≈ 13.85 dS m^{-1} near WP02). This pattern—higher EC where heads are below sea level and lower EC where heads are above MSL—is diagnostic of lateral seawater intrusion along the marine margin. Moderate EC at a few sites paired with strongly sub-MSL heads (e.g., WS05, WS06 near WP04) likely reflects mixing and transient recovery under variable pumping. In combination, the data indicate lateral encroachment near the coast and localized up-coning beneath high-demand cells inland. These observations underpin a conceptual intrusion model coupling head decline, lateral encroachment, and localized up-coning. A full density-dependent simulation (e.g., SEAWAT) is beyond the present scope but is prioritized for follow-up design of barriers/MAR placement.

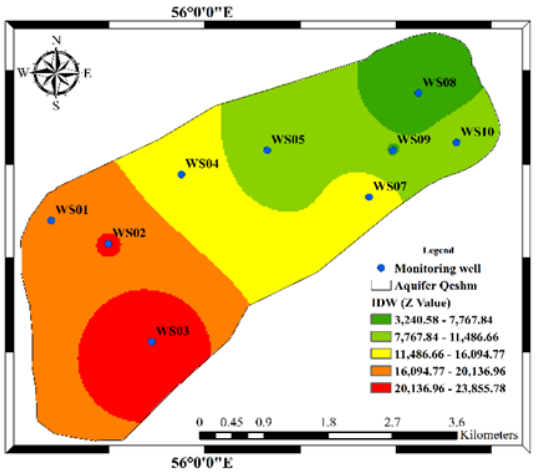

Figure 5. Annual average EC changes (monitoring wells)

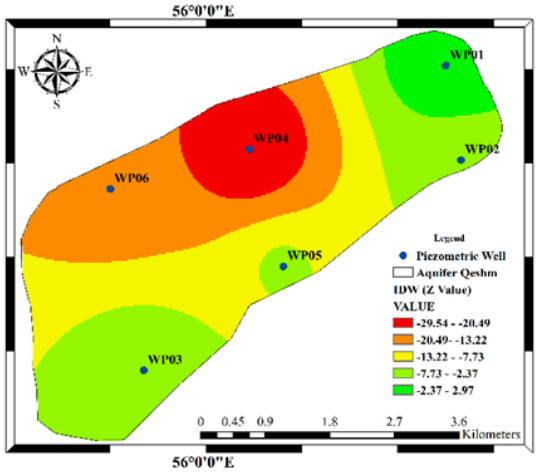

Figure 6. Annual average changes in groundwater-table elevation (piezometers)

The aggregated groundwater-level series shows a significant long-term decline (MK $\tau = -0.70$, $p < 0.001$); Sen's slope = − 0.084 m yr^{-1} (95% CI: − 0.116, − 0.061) over 2003 – 2018. The aggregated EC series shows an upward but not statistically significant trend

(MK $\tau = 0.16$, $p = 0.50$); Sen's slope ≈ +133 μS cm^{-1} yr^{-1} (≈ + 0.133 dS m^{-1} yr^{-1}; 95% CI: −82, +477) over 2007 – 2019 (see Table 6). Considering Per-well robustness, Piezometers WP03, WP05, and WP06 exhibit significant declines; WP01 rises modestly. Among quality wells, WS01 increases significantly in EC while WS04 decreases; others are mixed/non-significant. These per-well patterns are consistent with the aquifer-wide signal of drawdown and heterogeneous salinization (Table 7).

Table 6. Aquifer-wide (Thiessen-aggregated) trend statistics (MK and Sen)

Series (unit)	N (yrs)	Kendall's τ	p-value	Sen's slope (per year)	95% CI (Sen)
Groundwater level (m relative to MSL)	16	−0.70	<0.001	−0.084 m yr^{-1}	[−0.116, −0.061]
Electrical conductivity (μS cm^{-1})	11	+0.16	0.50	+133 μS cm^{-1} yr^{-1} (≈ +0.133 dS m^{-1} yr^{-1})	[−82, +477]

Note: *Annual series based on Thiessen-weighted aggregation over the aquifer.*

Table 7. Per-well MK/Sen highlights (wells with significant trends)

Well	Variable	N (yrs)	Kendall's τ	p-value	Sen's slope (per year)	Interpretation
WP03	Water level (m vs MSL)	16	−0.93	<0.001	−0.060 m yr^{-1}	Strong decline
WP05	Water level (m vs MSL)	16	−0.93	<0.001	−0.048 m yr^{-1}	Strong decline
WP06	Water level (m vs MSL)	16	−0.61	<0.001	−0.015 m yr^{-1}	Decline
WP01	Water level (m vs MSL)	16	+0.42	0.019	+0.034 m yr^{-1}	Modest rise
WS01	EC (μS cm^{-1})	11	+0.67	0.008	+41.7 μS cm^{-1} yr^{-1} (≈ +0.0417 dS m^{-1} yr^{-1})	EC increasing
WS04	EC (μS cm^{-1})	11	−0.64	0.019	−36.4 μS cm^{-1} yr^{-1} (≈ −0.036 dS m^{-1} yr^{-1})	EC decreasing

Note: *Only statistically significant trends shown here.*

3.5. Recharge, Storage, and Support Time of the Aquifer

Published subsurface investigations indicate that the unconsolidated sediment fill above the Tourian aquifer varies with topography ranged from 15 to 40 m in thickness, with independent surveys converged on an average depth-to-bedrock of 37 m across the plain [47]. The aquifer comprises coarse to medium-grained Quaternary gravels and sands with wide but overlapping porosity ranges [47] (gravels: 0.13–0.44; sands: 0.18–0.43 [48]). Taking the midpoint of the composite effective porosity window yields $\phi_e = 0.29$, and because specific retention in such coarse-grained materials is small (≈0.02–0.05; Minnesota Stormwater Manual), the true specific yield $S_y = \phi_e - S_r$ differs from ϕ_e by only a few hundredths. To maintain modest conservatism while acknowledging this small bias, we employ $S_y \approx 0.25$ for storage volume calculations (i.e., using ϕ_e as a proxy but reducing it slightly to hedge against overestimation). The aerial extent of the active aquifer is A=17.2 km^2. Thus, the recoverable groundwater storage under unconfined conditions is as follows:

$$V_{storage} = S_y \times B \times A$$
$$= 0.25 \times 37\ m \times 17.2 \times 10^6\ m^2$$
$$= 1.59 \times 10^8\ m^3$$

As noted in Section 3-1, the island mean annual precipitation is $P \approx 122$ mm yr^{-1}. Adopting a loss scenario of 70%, leaves roughly 30% of precipitation available for partitioning between surface runoff and any diffuse groundwater infiltration (i.e., the available budget ≈ 0.30 × 122 mm). Local hydrologic monitoring and watershed assessments indicate that, for this arid island, most of the limited post-evaporation precipitation is routed as surface runoff in the principal wadis, leaving little mass-balance room for substantial diffuse groundwater recharge *[49]*; *[50]*. On this basis we adopt a conservative minimal-recharge regime, consistent with hyper-arid settings where diffuse recharge is typically very small and effective inputs—when present—are focused beneath wadis. We therefore carry a sensitivity $R = \varepsilon AP$ with with $\varepsilon = 1\%\ and\ 2\%$ to bound plausible recharge while holding withdrawals constant. This justifies treating the aquifer as being in a regime where natural replenishment is minimal and the system is under net overdraft if withdrawals continue at rates exceeding whatever small diffuse recharge may occur.

To align volumetric depletion with observed heads, the net depletion was calibrated from the long-term groundwater-level trend using the baseline properties:

$$Q_{overdraft} \approx S_{y,base} \times A \times \Delta h$$
$$= 0.25 \times 17.2 \times 10^6\ m^2$$
$$\times\ 0.091\ m/yr$$
$$\approx 0.391 \times 10^6\ m^3/yr$$

Therefore, the corresponding support time is:

$$T = \frac{V_{storage}}{Q_{overdraft}} \approx \frac{1.59 \times 10^8}{0.391 \times 10^6} \approx 406.6\ years$$

(Including minimal recharge) at $\varepsilon = 1\%$ increases T to ~452 yr; at $\varepsilon = 2\%$, to ~510 yr (withdrawals held constant).

These results indicate that the Qeshm aquifer currently functions as a depleting reservoir: withdrawals in excess of minimal natural replenishment are buffered by finite storage. The support horizon may shorten or lengthen with changes in decline rate, climate, spatial heterogeneity in S_y and B, and extraction intensity. Sustained drawdown risks quality deterioration (e.g., salinity increases via up-coning or seawater intrusion) and a reduction in practically recoverable storage, underscoring the need to constrain abstraction and to consider managed replenishment where feasible.

3.5.1 Sensitivity of Storage and Support Time to S_y and B

Uncertainty in aquifer properties was propagated by sampling $S_y \in [0.18, 0.43]$ (step 0.01) and $B \in [15, 40]$ m (step 1 m). For each (S_y, B) pair, storage and support time were evaluated at the observed decline rate via Eqs. (4)–(5).

At the baseline (S_y = 0.25, B = 37 m), $V_{storage}$ = 159.1 Mm^3 and T = 406.6 yr. Holding B = 37 and varying S_y across 0.18–0.43 yields T = 292.8 to 699.3 yr (−28.0% to +72.0% relative to baseline). Holding S_y = 0.25 and varying B across 15–40 m yields T = 164.8 to 439.6 yr (−59.5% to +8.1%). The corresponding storage volumes and support times for these representative (S_y, B) pairs are listed in Table 8. The one-at-a-time response is summarized in Figure 7, while the full two-parameter surface $T(S_y, B)$ is shown in Figure 8. The near-linear response in each parameter, combined with the broader geological range in B, explains the larger fractional sensitivity at low thicknesses. These results indicate that plausible parameter uncertainty can shift the support horizon by several centuries under the present long-term decline, motivating targeted field tests (e.g., slug or pumping tests and additional logs) to narrow S_y and B.

Table 8. Sensitivity of recoverable storage $V_{storage}$ and support time T to S_y and B

S_y	B (m)	$V_{storage}$ (Mm³)	T at 0.091 m·yr⁻¹ (yr)
0.18	15	46.44	118.68
0.18	25	77.40	197.80
0.18	37	114.55	292.75
0.18	40	123.84	316.48
0.25	15	64.50	164.84
0.25	25	107.50	274.73
0.25	**37**	**159.10**	**406.59**
0.25	40	172.00	439.56
0.43	15	110.94	283.52
0.43	25	184.90	472.53
0.43	37	273.65	699.34
0.43	40	295.84	756.04

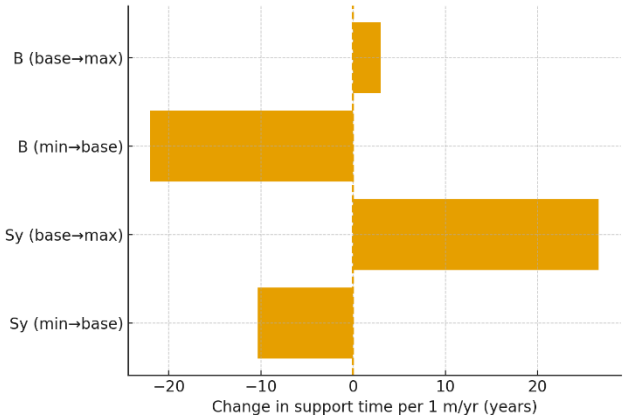

Figure 7. One-at-a-time sensitivity of support time to aquifer properties

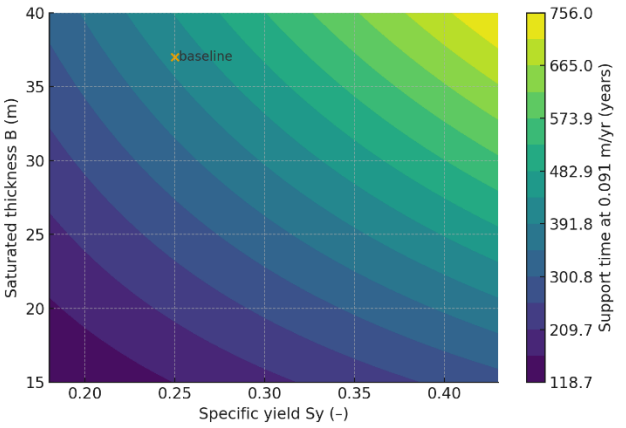

Figure 8. Two-parameter response surface of support time $T(S_y, B)$

3.6. Salinity Constraints and Adaptive Use Options for Groundwater in Qeshm Island

The aggregated electrical conductivity of the Qeshm Island aquifer (~14,000 µS/cm, ≈14 dS/m at 25 °C) places the resource well beyond agronomic acceptability under conventional irrigation. According to recent literature, waters with ECw above ~3 dS/m face severe use restrictions due to salinity hazards [51]. Only highly salt-tolerant species such as date palm (Phoenix dactylifera), which has been tested under irrigation salinities up to ~15 dS/m, and certain halophytic grains like quinoa and amaranth might survive, although even these exhibit yield or quality reductions without careful management [52]; [53]; [54]. Thus, sustainable irrigation with such saline groundwater requires deliberate practices: implementing a leaching fraction (often on the order of 20%–40% above crop evapotranspiration) to prevent root-zone salt buildup and employing localized

delivery systems (e.g., drip or subsurface irrigation) to minimize surface salt concentration and optimize water use efficiency [55]; [56]; [57] Beyond conventional agriculture, Qeshm Island's high-salinity groundwater can be repurposed in niche or engineered systems where elevated dissolved solids are acceptable or advantageous. Brackish aquaculture species, including tilapia and select penaeid shrimp, tolerate salinities in the approximate range of 8–14 ppt (≈8–14 dS/m), enabling production without full desalination [58]. Similarly, cultivation of halotolerant microalgae or cyanobacteria—photosynthetic organisms that thrive at elevated salinity and can be cultivated in brackish water to produce lipids, pigments, and feed additives—for biofuel precursors, feedstock, or other bioproducts can exploit saline media to suppress freshwater contaminants while leveraging organisms adapted to osmotic stress [59]. Alternatively, dissolved minerals in groundwater can be recovered via controlled crystallization (e.g., NaCl, gypsum), converting high total dissolved solids into marketable by-products, adding an extractive-value dimension to resource utilization [49].

The native conductivity is prohibitive for most other end uses including potable supply, boiler feedwater, cooling-tower makeup, and many industrial processes. Industrial and boiler water quality standards commonly require much lower EC (e.g., <0.2–2 dS/m depending on application), necessitating blending with fresher sources or pretreatment through membrane processes such as reverse osmosis or electrodialysis; these methods reduce conductivity but incur energy and concentrate-management costs [60]; [40]. Untreated brackish water may be directly usable in lower-quality-demand applications, such as certain geothermal or oilfield injection schemes, avoiding the resource and waste burdens of intensive treatment [61].

In summary, while the aquifer's inherent salinity severely restricts broad-scale conventional irrigation and direct potable/industrial use, strategic crop selection, adaptive irrigation management, and alternative utilization pathways can enable beneficial exploitation. The sustainable development of the resource should integrate ongoing monitoring of salinity and head changes and consider the coupling between declining water table elevations and salinization mechanismssuch as seawater intrusion or up-coningso as to preempt irreversible degradation.

4. Conclusion

This Gulf-margin aquifer is a coastal system subject to marine boundary controls; water-supply planning is therefore a marine-oriented engineering problem as much as a hydrologic one. Within this hyper-arid coastal setting, vulnerability is shaped as much by parameter uncertainty in aquifer properties as by demand growth.

The Renewable Water per Capita (RWRPC) analysis reveals that demographic growth more than any systematic decline in precipitation is the principal driver pushing the island toward water vulnerability and, under business-as-usual trajectories, scarcity. Even with conservative assumptions about extractable renewable supply (e.g., a 40% sustainable withdrawal fraction), projected per-capita availability declines sharply, falling into the "vulnerable" category in the near term and approaching "scarce" levels by 2036 (≈757 m^3 pp yr^{-1}) unless growth, consumption patterns, or allocation strategies are altered. The 70/20/10 policy benchmark is used as a neutral comparator anchored in global withdrawal shares. Under the mixed-allocation scenario examined (70% agriculture, 20% industry, 10% domestic), the island's renewable supply could support roughly 1,523 ha of date palms, sustain industrial output at the order of 3.35×10^5 t yr^{-1} and water supply for ≈23,841 residents, while generating approximately $351.4 million in combined annual revenues illustrating that, even when allocated conservatively, the resource can enable sizeable economic activity but only if extraction is constrained to sustainable bounds. When paired with sectoral capacity estimates, these RWRPC projections illustrate a narrowing window for supporting population and economic expansion without either overstepping sustainable limits or imposing significant demand-side restrictions.

The hydrologic budget and groundwater analyses contextualize this demographic pressure within the buffering and limits of the physical system. The surface water balance across the six principal watersheds shows that approximately 60% of precipitation is returned to the atmosphere, with runoff consuming nearly all of the non-evaporative remainder leaving little detectable natural recharge to the underlying Tourian aquifer. Consequently, the declining water table (reflecting an overdraft of ~0.091 m/yr) signals reliance on stored groundwater. Conservative storage estimates, based on representative thickness, extent, and specific yield, place the recoverable volume at 1.5 × 10^8 m^3. At the observed decline rate Δh = 0.091 m yr^{-1}, this corresponds to a support horizon of ~406.6 years; under plausible ranges in S_y and B, the horizon spans ~165–756 years. The buffer is therefore finite and uncertain: it can accommodate shocks temporarily but cannot sustain unconstrained demand growth without management.

Simultaneously, the groundwater quality is deteriorating: rising electrical conductivity into the high-brackish range (~14–16.6 dS/cm) constrains the direct use and conventional irrigation options. The co-occurrence of head decline and increasing salinity implies coupled stress processes such as diminished hydraulic resistance enabling up-coning or saline intrusion that progressively degrade the effective usable resource beyond mere volumetric depletion. For

process-critical industrial uses (e.g., boiler/cooling makeup), acceptable water typically requires low salinity (conductivity on the order of ≈ 0.2–2 dS m^{-1}) with low hardness and silica; continued salinization therefore reduces the feasibility of meeting such demands without treatment or blending. Thus, quantity and quality are not independent constraints but reinforcing feedbacks, magnifying the risk of crossing thresholds that would sharply reduce both availability and utility. Meanwhile, observed high EC co-located with sub-MSL heads at nearby piezometers supports a lateral intrusion control along vulnerable shorelines, while deeper inland cells with moderate EC under strong drawdown remain candidates for up-coning. Prior to engineering intervention, a targeted major-ion program (for Piper/Stiff facies) and depth-profiled EC & head at a subset of coastal and inland wells will sharpen diagnosis and optimize placement of any hydraulic barrier or MAR elements.

Treated wastewater (TWW) represents a strategic, marine-compatible source for non-potable demands and seasonal MAR. Routing tertiary TWW to wadi-adjacent infiltration basins or vadose-zone wells can build a freshwater mound inland of vulnerable shorelines, enhancing the hydraulic barrier while supplying irrigation or industrial cooling via fit-for-purpose quality targets. Implementation requires routine monitoring (EC, nutrients, pathogens, trace organics) and clear operational triggers aligned with the head- and EC-based management bands.

The RWRPC trends, minimal recharge, storage depletion, and salinization constitute a compound risk to the island's water resilience. Therefore, sustainable management must be multi-dimensional. Immediate imperatives include aligning extraction with the sum of renewable and buffered (stored) capacity to arrest overdraft, instituting continuous head and salinity monitoring with pre-defined action thresholds, for example, head-decline action bands (e.g., 3-year rolling slope exceeding a set limit) and EC thresholds linked to domestic/irrigation/industrial usability classes, and embedding demand-side controls such as efficiency measures, allocation prioritization, and possibly adaptive pricing to moderate per capita consumption in line with realistic availability. Supply-side adaptation should not rely solely on conventional expansion: saline groundwater, while unsuitable for many direct uses, can support niche or engineered applications (e.g., halotolerant agriculture, brackish aquaculture, or mineral extraction), whereas higher quality requirements must be met through blending or selective treatment with transparent accounting for energetic and disposal costs. From a coastal-engineering perspective, candidate measures include subsurface beach-well intakes to improve raw-water quality for desalination pre-treatment, selective hydraulic barriers (well arrays) at vulnerable shorelines where heads drop below sea level, and conjunctive use that shifts non-potable demands to brackish sources while protecting inland fresh pockets. These measures should be triggered by head-decline and EC action bands defined for coastal aquifers.

This assessment is subject to several limitations and working assumptions that frame interpretation of the results. Trend statistics were evaluated with Mann–Kendall and Sen's slope on Thiessen-aggregated annual series, with per-well tests reported for wells with ≥8 years; confidence intervals reflect the non-parametric Helsel–Hirsch approach. Aquifer properties were represented by a baseline S_y = 0.25 and B = 37 m (range 15–40 m), and while our parameter sweep shows support times spanning 165–756 yr at the observed decline rate (Section 3.5.1; Figs. 7,8; Table 8), field measurements (slug/pumping tests and additional logs) are needed to narrow these bounds and resolve lateral/vertical heterogeneity not captured by the lumped calculations. The monitoring network is intentionally coarse (piezometers and EC wells spaced ~1.1–1.7 km median within the 17.2 km^2 aquifer; rainfall stations ~11–45 km island-wide), adequate for basin-scale diagnostics but not for fine-scale mapping; denser coastal transects and one inland depth-profiled site would materially reduce spatial uncertainty. Long-term depletion $Q_{overdraft}$ was calibrated from the groundwater-level trend Δh = 0.091 m yr^{-1} using baseline S_y and area because well- or field-level pumpage records were unavailable; the estimate therefore represents net stress (withdrawals minus recharge) and assumes stationarity over the analysis window, with interannual variability in withdrawals and climate not explicitly modeled. Net natural recharge was treated as negligible based on the arid water-budget and runoff routing, which is conservative but may overlook localized or episodic diffuse inputs in rare wet years. To reconcile the surface-water budget with aquifer dynamics, we bracketed minimal net diffuse recharge with ε = 1–2% of precipitation in sensitivity tests; these bounds modestly extend support time without altering the qualitative conclusions. Water-quality interpretation relies on EC as a salinity proxy; temperature normalization, ionic composition, and density-driven flow processes (e.g., up-coning, seawater intrusion) were not simulated and could affect practical recoverability during continued drawdown. Aggregated EC shows a weak, non-significant upward trend, while per-well tests indicate heterogeneous behavior (significant increases at some coastal sites and decreases at others), consistent with mixed lateral intrusion and up-coning; targeted major-ion sampling (for Piper/Stiff facies) and depth-profiled EC/head are needed to resolve mechanisms prior to engineering intervention. Sector capacities and revenues use fixed coefficients from Section 3.3; technological change or policy shifts would alter these yields. Reported revenues are gross (not net of O&M or energy), use

constant unit values for policy comparison, and are robust to ±25% unit-price variations without changing scenario ranking; future scenarios should include price/productivity sensitivity and explicit costs for treatment and disposal. Finally, the 70/20/10 allocation is employed as a policy benchmark anchored in global withdrawal shares, not as a claim about current local use.

Finally, while this study provides a defensible first-order synthesis integrating demographic projections, water-budget accounting, aquifer storage/support estimation, and salinity dynamics reducing uncertainty in key parameters would strengthen future planning. Priorities for refinement include quantifying any low-level diffuse recharge, spatially resolving heterogeneity in storage properties and extraction patterns, and stress testing RWRPC projections under alternate demographic or policy scenarios. An integrated governance framework that explicitly couples population growth, resource allocation (via RWRPC-aware planning), and subsurface feedbacks is essential to extend the sustainable water horizon of Qeshm Island, avoid irreversible degradation, and reconcile development ambitions with the physical limits of its hydrologic system. Targeted S_y testing and updated thickness mapping offer the fastest path to shrinking the planning window, while the 70/20/10 benchmark should continue to serve as a transparent comparator for allocation choices rather than a claim about present-day use.

5. References

1- JACKSON, R. B., CARPENTER, S. R., DAHM, C. N. and ET AL.,(2001), *Water in a changing world,* Ecological Applications, 11, p. 1027–1045.

2-YOUNG, M. E., (2004), in *Water Encyclopedia,* J. H. Lehr & J. Keeley Ed^Eds, Wiley, p. 470–474.

3-KHIYAT, Z.,(2022), *Groundwater in the Arab region: Making the invisible visible,* Desalination and Water Treatment, 263, p. 204–206.

4-HAN, J., (2016), *The analysis and prediction of water supply and demand for Beijing in future*, aper presented at the Conference Name|, Conference Location|, Date|.

5-ALAM, S., GEBREMICHAEL, M., LI, R., DOZIER, J. and LETTENMAIER, D.,(2020), *Can managed aquifer recharge mitigate the groundwater overdraft in California's Central Valley?,* Water Resources Research, 56, p. e2020WR027244.

6-RAY, P. A., KIRSHEN, P. H., ROSENBERG, D. E. and HAGAN, R. E., (2010), *An overview of the water situation in Amman, Jordan*, aper presented at the Conference Name|, Conference Location|, Date|.

7-MAGAR, S. S., (2006), *Best practices and technologies for agricultural water management*, aper presented at the Conference Name|, Conference Location|, Date|.

8-KHEIRINEJAD, S., BOZORG-HADDAD, O., SINGH, V. P. and LOÁICIGA, H. A.,(2022), *The effect of reducing per capita water and energy uses on renewable water resources in the water–food–energy nexus,* Scientific Reports, 12, p. 7582.

9-TYABO, A. M., OTACHE, M. Y., MUSA, J. J. and CHADO, A. S.,(2021), *Potential impacts of climate change and population growth on water resources in Guinea Savanna ecological zone of Nigeria,* The International Journal of Science & Technoledge, 9, p. 14–22.

10-DUARTE, R., PINILLA, V. and SERRANO, A., (2020), in *Water resources and economic processes,* Ed^Eds, Routledge.

11-ZHU, X., HOU, M. and WEI, J.,(2024), *Global water use and its changing patterns: Insights from OECD countries,* Water, 16, p. 3592.

12-LEE, J., NEMATI, M., ALLAIRE, M. and DINAR, A.,(2024), *The impact of pricing structure change on residential water consumption: A long-term analysis of water utilities in California,* Water Resources Economics, 46, p. 100240.

13-BOLORINOS, J., RAJAGOPAL, R. and AJAMI, N. K.,(2021), *Mining the gap in long-term residential water and electricity conservation,* Environmental Research Letters, 16, p. 024007.

14-GOBER, P., (2019), in *Population, place, and spatial interaction: Essays in honor of David Plane,* R. S. Franklin Ed^Eds, Springer, p. 249–260.

15-FARRAH, N. and WALRAEVENS, K., (2010), *Implication of salinity sources, geochemical evaluation and upper aquifer characterisation of Jifarah Plain, NW-Libya*, aper presented at the Conference Name|, Conference Location|, Date|.

16-BORROK, D. and BROUSSARD, W.,(2016), *Long-term geochemical evaluation of the coastal Chicot Aquifer System, Louisiana, USA,* Journal of Hydrology, 533, p. 320–331.

17-CRUZ-FUENTES, T., CABRERA, M., HEREDIA, J. and CUSTODIO, E.,(2014), *Groundwater salinity and hydrochemical processes in the volcano-sedimentary aquifer of La Aldea, Gran Canaria, Canary Islands, Spain,* Science of the Total Environment, 484, p. 154–166.

18-DUQUE, C., OLSEN, J., SÁNCHEZ-ÚBEDA, J. P. and CALVACHE, M., (2018), in *Advances in groundwater governance,* Ed^Eds, CRC Press, p. 117–126.

19-GUO, Z., FOGG, G. E., CHEN, K., PAULOO, R. and ZHENG, C.,(2022), *Sustainability of regional groundwater quality in response to managed aquifer recharge,* Water Resources Research, 59, p. e2021WR031459.

20-MILLER, K., FISHER, A. and KIPARSKY, M.,(2021), *Incentivizing groundwater recharge in the*

Pajaro Valley through Recharge Net Metering (ReNeM), Case Studies in the Environment.
21-MASKEY, M., *et al.*,(2022), *Managing aquifer recharge to overcome overdraft in the Lower American River, California, USA*, Water, 14(6), p. 966.
22-MARTÍNEZ-GRANADOS, D. and CALATRAVA, J.,(2014), *The role of desalinisation to address aquifer overdraft in SE Spain*, Journal of Environmental Management, 144, p. 247–257.
23-GORJIAN, S. and GHOBADIAN, B.,(2015), *Solar desalination: A sustainable solution to water crisis in Iran*, Renewable and Sustainable Energy Reviews, 48, p. 571–584.
24-NESTEROV, O.,(2025), *An assessment of seawater desalination impact on salinities in the Arabian/Persian Gulf using a 3D circulation model*, Ocean Modelling, 194, p. 102503.
25-RAFIEE, H. and BALOVI, F.,(2017), *Paradox of limited water resources in Iran and goals of self-sufficiency in agricultural sector*, Preprints.
26-SAEMIAN, P., TOURIAN, M. J., AGHAKOUCHAK, A. and ET AL.,(2022), *How much water did Iran lose over the last two decades?*, Journal of Hydrology: Regional Studies, 41, p. 101095.
27-TEIMOORI, M., MIRDAMADI, S. M. and HOSSEINI, S. J.,(2018), *Modeling of climate change effects on groundwater resources: The application of dynamic systems approach*, International Journal of Agricultural Management and Development, 9, p. 107–118.
28-SHARAFATI, A., ASADOLLAH, S. B. H. S. and SHAHBAZI, A.,(2021), *Assessing the impact of climate change on urban water demand and related uncertainties: A case study of Neyshabur, Iran*, Theoretical and Applied Climatology, 145, p. 473–487.
29-ZAKERI, M. A., MIRNIA, S. K. and MORADI, H.,(2022), *Assessment of water security in the large watersheds of Iran*, Environmental Science & Policy, 127, p. 31–37.
30-REZAEI, A., *et al.*,(2019), *Evaluation of groundwater quality and heavy metal pollution indices in Bazman basin, southeastern Iran*, Groundwater for sustainable development, 9, p. 100245.
31-GHIASSI, R. and ZEYNOLABEDIN, A.,(2019), *A standardized index for assessing seawater intrusion in coastal aquifers: The SIVI index*, Environmental Earth Sciences, 78, p. 666.
32-ZEYNOLABEDIN, A., GHIASSI, R. and DOLATSHAHI PIROOZ, M.,(2021), *Seawater intrusion vulnerability evaluation and prediction: a case study of Qeshm Island, Iran*, Journal of Water and Climate Change, 12(1), p. 265–277.
33-CHITSAZAN, M. and ET AL.,(2017), *Hydrogeological investigation of Qeshm Island*, Environmental Earth Sciences, 76(14).
34-ZIAEI, M. and ET AL.,(2021), *GALDIT assessment of Qeshm*, Environmental Earth Sciences, 80(15).
35-SEDGHI, M. M. and ZHAN, H.,(2020), *Groundwater flow modeling*, Journal of Hydrology, 584, p. 124662.
36-PAPARELLA, F., D'AGOSTINO, D. and BURT, J. A.,(2022), *Long-term, basin-scale salinity impacts from desalination in the Arabian/Persian Gulf*, Scientific Reports, 12, p. 20549.
37-FAO, (2023), *AQUASTAT - FAO's Global Information System on Water and Agriculture*.
38-UNESCO, (2024), *Statistics | UN World Water Development Report*.
39-INGRAO, C., STRIPPOLI, R., LAGIOIA, G. and HUISINGH, D.,(2023), *Water scarcity in agriculture: An overview of causes, impacts and approaches for reducing the risks*, Heliyon, 9(8), p. e18507.
40-AGENCY, U. S. E. P., (2015), *Secondary drinking water standards: Guidance for nuisance chemicals (EPA 816-F-15-002)*, U.S. EPA.
41-HEALY, R. W., WINTER, T. C., LABAUGH, J. W. and FRANKE, O. L., (2007), *Water budgets: Foundations for effective water-resources and environmental management (USGS Circular 1308)*, U.S. Geological Survey.
42-TODD, D. K.,(2008), *Groundwater Hydrology*, Wiley.
43-KONIKOW, L. F. and BREDEHOEFT, J. D.,(2020), *Groundwater Resource Development: Effects and Sustainability*, The Groundwater Project.
44-NOORI, R., *et al.*,(2023), *Decline in Iran's groundwater recharge*, Nat Commun, 14(1), p. 6674.
45-LAZZARINI, M., MOLINI, A., MARPU, P. R., OUARDA, T. B. M. J. and GHEDIRA, H.,(2015), *Urban climate modifications in hot desert cities: The role of land cover, local climate, and seasonality*, Geophysical Research Letters, 42(22), p. 9980–9989.
46-HOSSEINYAR, G., BEHBAHANI, R., MOUSSAVI-HARAMI, R., LAK, R. and KUIJPERS, A.,(2021), *Holocene sea-level changes of the Persian Gulf*, Quaternary International, 571, p. 26–45.
47-ZEYNOLABEDIN, A. and GHIASSI, R.,(2019), *The SIVI index: a comprehensive approach for investigating seawater intrusion vulnerability for island and coastal aquifers*, Environmental Earth Sciences, 78(24), p. 666.
48-WOESSNER, W. W. and POETER, E. P.,(2020), *Hydrogeologic Properties of Earth Materials and Principles of Groundwater Flow*, The Groundwater Project.
49-LOGANATHAN, P., VIGNESWARAN, S., KANDASAMY, J. and NAIDU, R.,(2006), *Use of renewable energy for desalination: Implications for developing countries*, Desalination, 192(1-3), p. 1–16.
50-JIANG, Y.,(2015), *China's water security: Current status, emerging challenges and future prospects*, Environmental Science & Policy, 54, p. 106–125.
51-PAZ, A. M., *et al.*,(2023), *Salt-affected soils: Field-scale strategies for prevention, mitigation, and*

adaptation to salt accumulation, Italian Journal of Agronomy, 18(2), p. 2166.
52-AL-DAKHEEL, A. J., HUSSAIN, M. U. R. I., ABDULRAHMAN, A. and ABDULLAH, A.-H.,(2022), *Long-term assessment of salinity impact on fruit yield in eighteen date palm varieties*, Agricultural Water Management, 269, p. 107683.
53-HAMMAMI, Z., MAHMOUDI, H., AL JANAAHI, A. and SINGH, R. K.,(2024), *Evaluation of date palm fruits quality under different irrigation water salinity levels compared to the fruit available in the market*, Frontiers in Sustainable Food Systems, 7, p. 1322350.
54-CHAGANTI, V. N. and GANJEGUNTE, G. K.,(2024), *Quinoa growth and yield performance under salinity stress in arid West Texas*, Agrosystems, Geosciences & Environment, 7(2), p. e20493.
55-SHAHROKHNIA, H. and WU, L.,(2021), *SALEACH: A new web-based soil salinity leaching model for improved irrigation management*, Agricultural Water Management, 252, p. 106905.
56-WANG, Y.,(2023), *Soil moisture and salinity dynamics of drip irrigation in saline-alkali soil of Yellow River Basin*, Frontiers in Environmental Science, 11, p. 1130455.
57-TAROLLI, P., LUO, J., PARK, E., BARCACCIA, G. and MASIN, R.,(2024), *Soil salinization in agriculture: Mitigation and adaptation strategies combining nature-based solutions and bioengineering*, iScience, 27, p. 108830.
58-LIGHTNER, D. V.,(2011), *Virus diseases of farmed shrimp in the Western Hemisphere (the Americas): A review*, Journal of Invertebrate Pathology, 106(1), p. 110–130.
59-ZHANG, S., ZHANG, L., XU, G., LI, F. and LI, X.,(2022), *A review on biodiesel production from microalgae: Influencing parameters and recent advanced technologies*, Frontiers in Microbiology, 13, p. 970028.
60-ENGINEERS, A. S. O. M., (2019), *ASME guidelines for watertube boilers*, ASME.
61-KHARAKA, Y. K., AMBATS, G. and THORDSEN, J. J., (2006), in *Groundwater geochemistry and its application to subsurface flow studies*, p. 45–64.